A High-Accuracy Realization of the Yee Algorithm Using Non-Standard Finite Differences

James B. Cole, *Member, IEEE*

***Abstract*— New nonstandard second-order finite differences (FD's) are introduced, which when substituted into the Yee algorithm, reduce the solution error by a factor of 10^{-4} on a coarse computational grid. Using λ/h (grid spacings per wavelength) $= 8$, one achieves the same accuracy as the standard Yee algorithm does at $\lambda/h = 1140$. In addition, greater algorithmic stability allows a reduction in the number of iterations needed to solve a problem.**

***Index Terms*—FDTD, nonstandard finite-difference, Maxwell's equations, Yee algorithm.**

I. Introduction

THE ACCURACY of the second-order finite-difference time-domain (FDTD) algorithm developed by Yee [1] to solve Maxwell's equations is low, unless a fine grid is used, which imposes high computational costs. Higher order finite-difference (FD) approximations could be employed, but this not only increases computational costs, but also complicates the algorithm. In this paper, the nonstandard FD (NSFD) concepts introduced by Mickens [2] are extended to construct a high-accuracy version of the Yee algorithm based on NSFD's. At the expense of a modest increase in algorithmic complexity, it is possible to achieve a large increase in accuracy subject to certain constraints, which can be wholly or partially circumvented.

This paper's algorithm has been implemented in parallel FORTRAN code and used to model spatially variant media and irregular boundaries. By displaying one or more fields per wave period, one obtains animated visualizations of time-dependent electromagnetic scattering and propagation processes during the computation without the need to store large data sets.

II. NSFD's

The standard second-order central FD approximation to the first derivative is given by

$$\mathbf{d}_x f(x) = \frac{\tilde{\mathbf{d}}_x f(x)}{\Delta x} \tag{1}$$

where $\tilde{\mathbf{d}}_x$ is a difference operator defined by $\tilde{\mathbf{d}}_x f(x) = f(x + \Delta x/2) - f(x - \Delta x/2)$. An NSFD [2] is defined by

$$\mathbf{d}_x^{\mathrm{ns}} f(x) = \frac{\tilde{\mathbf{d}}_x f(x)}{s(\Delta x)} \tag{2}$$

where s is a correction function chosen to minimize the difference $|(\partial_x - \mathbf{d}_x^{\mathrm{ns}}) f(x)|$ with respect to some set of basis functions. In special cases it is even possible to construct exact FD algorithms. While it is impossible to construct an exact second-order FD algorithm to solve Maxwell's equations in two and three dimensions, it is possible to greatly improve the accuracy of the Yee algorithm using the new second-order NSFD's which are introduced in this paper, following the methodology developed in [3].

III. Standard Yee Algorithm

To define this paper's approach, we first consider TM solutions ($E_x = E_y = 0$, $E_z \neq 0$; $H_x \neq 0$, $H_y \neq 0$, $H_z = 0$) to the two-dimensional (2-D) sourceless Maxwell's equations in a nonconducting medium. Maxwell's equations

$$\mu(\mathbf{x})\partial_t \mathbf{H}(\mathbf{x},t) = -\nabla \times \mathbf{E}(\mathbf{x},t) \tag{3a}$$

$$\varepsilon(\mathbf{x})\partial_t \mathbf{E}(\mathbf{x},t) = \nabla \times \mathbf{H}(\mathbf{x},t) \tag{3b}$$

then reduce to

$$\mu(\mathbf{x})\partial_t H_x(\mathbf{x},t) = -\partial_y E_z(\mathbf{x},t) \tag{4a}$$

$$\mu(\mathbf{x})\partial_t H_y(\mathbf{x},t) = \partial_x E_z(\mathbf{x},t) \tag{4b}$$

$$\varepsilon(\mathbf{x})\partial_t E_z(\mathbf{x},t) = \partial_x H_y(\mathbf{x},t) - \partial_y H_x(\mathbf{x},t) \tag{4c}$$

where $\mathbf{x} = (x, y)$ is a position vector, and $\varepsilon(\mathbf{x})$ and $\mu(\mathbf{x})$ are local dielectric permittivity and magnetic permeability, respectively.

Replacing the derivatives in (4) by standard FD's, one obtains a realization of the Yee algorithm

$$\tilde{\mathbf{d}}_t H_x\left(x, y - \frac{h}{2}, t\right) = \frac{-1}{\mu(\mathbf{x})}\frac{\Delta t}{h}\tilde{\mathbf{d}}_y E_z\left(x, y - \frac{h}{2}, t\right) \tag{5a}$$

$$\tilde{\mathbf{d}}_t H_y\left(x - \frac{h}{2}, y, t\right) = \frac{1}{\mu(\mathbf{x})}\frac{\Delta t}{h}\tilde{\mathbf{d}}_x E_z\left(x - \frac{h}{2}, y, t\right) \tag{5b}$$

$$\tilde{\mathbf{d}}_t E_z\left(x, y, t + \frac{\Delta t}{2}\right) = \frac{1}{\varepsilon(\mathbf{x})}\frac{\Delta t}{h}\left[\tilde{\mathbf{d}}_x H_y\left(x, y, t + \frac{\Delta t}{2}\right) - \tilde{\mathbf{d}}_y H_x\left(x, y, t + \frac{\Delta t}{2}\right)\right]. \tag{5c}$$

For simplicity, one sets $\Delta x = \Delta y = h$. An explicit FDTD algorithm is obtained by solving for quantities which contain $t + \frac{\Delta t}{2}$ or $t + \Delta t$ on the left.

IV. Solution Error

The solution error and stability of algorithm (5) are analyzed [4] by considering plane-wave solutions for a field component of the form $\psi_0(\mathbf{x}, t) = Ae^{i(\mathbf{k}\cdot\mathbf{x} - \omega t)}$ in a uniform medium

Manuscript received January 22, 1997; revised February 28, 1997.

The author is with the Institute for Information Science and Electronics, University of Tsukuba, Tsukuba, Japan 305, on leave from the Naval Research Laboratory, Washington, DC 20375-5337 USA.

Publisher Item Identifier S 0018-9480(97)03924-0.

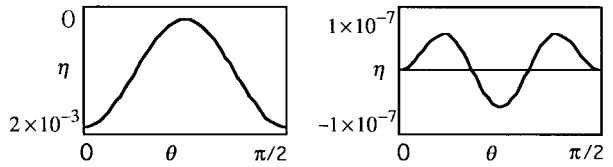

(a) (b)

Fig. 1. Solution error for (a) the standard Yee algorithm, and (b) its high-accuracy version for a plane wave propagating at angle θ, with respect to the x-axis. Spatial grid is $\lambda/h = 8$, with $T/\Delta T = 12$, where λ and T are the wavelength and wave period, respectively.

$(\varepsilon(\mathbf{x}), \mu(\mathbf{x}) = \text{constant})$, where $\mathbf{k} = (k_x, k_y) = k(\cos\theta, \sin\theta)$. Maxwell's equations then reduce to the wave equation with respect to each field component

$$(\partial_{tt} - v^2\nabla^2)\psi(\mathbf{x}, t) = 0 \tag{6}$$

while (5) reduces to the FD approximation of (6)

$$(\mathbf{d}_{tt} - v^2\mathbf{D}^2)\psi(\mathbf{x}, t) \tag{7}$$

where $\mathbf{d}_{tt} = \mathbf{d}_t\mathbf{d}_t$, $\mathbf{D}^2 = \mathbf{d}_{xx} + \mathbf{d}_{yy}$ is a FD Laplacian operator, $v = 1/\sqrt{\varepsilon\mu}$ is the wave velocity, and ω, the angular frequency, and k, the wave number, satisfy the dispersion relation $\omega/k = v$.

Inserting $\psi_0(\mathbf{x}, t)$ into (7), one defines the solution error η by

$$\left(\mathbf{d}_{tt} - v^2\mathbf{D}^2_{(1)}\right)\psi_0(\mathbf{x}, t) = 4\eta(\omega, \mathbf{k})\psi_0(\mathbf{x}, t) \tag{8}$$

and obtains

$$\eta(\omega, \mathbf{k}) = -\frac{1}{\Delta t^2}\sin^2(\omega\Delta t/2) + \frac{1}{h^2}v^2(\sin^2(k_x h/2) + \sin^2(k_y h/2)). \tag{9}$$

A plot of η as a function of the propagation direction θ (at fixed $k = |\mathbf{k}|$) is shown in Fig. 1(a). Notice the large directional anisotropy.

Following [2], one might try to eliminate the solution error by replacing the standard FD's in (5) with NSFD's defined by

$$\mathbf{d}^{\text{ns}}_\xi = \frac{1}{s_a(\Delta\xi)}\tilde{\mathbf{d}}_\xi \tag{10}$$

where the function

$$s_a(\Delta\xi) = 2\sin(a\Delta\xi/2)/a \tag{11}$$

is chosen such that $\mathbf{d}^{\text{ns}}_\xi e^{ia\xi} = \partial_\xi e^{ia\xi}$ exactly. Unfortunately, the definition of the spatial NSFD's is directionally anisotropic, which means that one can construct a zero-error FD algorithm only with respect to plane waves propagating in the particular direction $\mathbf{k} = (k_x, k_y)$, for which the $\mathbf{d}^{\text{ns}}_\xi$ are defined. Such an algorithm is of little practical value.

V. Nonstandard FD Spatial-Derivative Operators

In [3] a nearly isotropic FD Laplacian $\mathbf{D}^2_{(0)}$ was introduced, for which

$$\mathbf{D}^2_{(0)}\psi_0(\mathbf{x}, t) \cong \nabla^2\psi_0(\mathbf{x}, t) \tag{12}$$

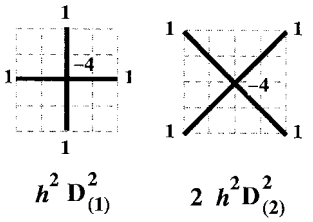

(a) (b)

Fig. 2. Graphical depiction of two independent FD approximations to the Laplacian in two dimensions. Each figure, centered at (x, y), represents a summation. Grid spacing is $h/2$. Vertices represent the value of a function at the corresponding geometrical position, and the numbers indicate its summation weight.

is an excellent approximation for all values of θ. $\mathbf{D}^2_{(0)}$ is constructed by superposing two standard FD Laplacians

$$s_k(h)^2\mathbf{D}^2_{(0)} = \gamma_0 h^2\mathbf{D}^2_{(1)} + (1-\gamma_0)h^2\mathbf{D}^2_{(2)} \tag{13}$$

where $\mathbf{D}^2_{(1)} = \mathbf{D}^2$ and $\mathbf{D}^2_{(2)}$ are given by

$$h^2\mathbf{D}^2_{(1)}f(x,y) = [f(x+h,y) + f(x-h,y) + f(x,y+h) + f(x,y-h)] - 4f(x,y) \tag{14a}$$

$$h^2\mathbf{D}^2_{(2)}f(x,y) = \frac{1}{2}[f(x+h,y+h) + f(x+h,y-h) + f(x-h,y+h) + f(x-h,y-h)] - 2f(x,y). \tag{14b}$$

$\mathbf{D}^2_{(1)}$ and $\mathbf{D}^2_{(2)}$ are graphically depicted in Fig. 2. The superposition parameter γ_0 is given by

$$\gamma_0(k) = \left.\frac{\cos k_x\cos k_y - \cos k}{1 - \cos k_x\cos k_y - \cos k_x - \cos k_y}\right|_{(k_x,k_y)=k(\cos\theta_0,\sin\theta_0)} \tag{15}$$

where $\theta_0 = 0.182\,03\pi$.

If NSFD derivative operators $\mathbf{d}'_x$ and $\mathbf{d}'_y$ could be determined, such that $\mathbf{D}^2_{(0)} = \mathbf{d}'_x\mathbf{d}'_x + \mathbf{d}'_y\mathbf{d}'_y$, one could construct a high-accuracy version of the Yee algorithm. Unfortunately one cannot realize this decomposition, but one can write

$$s_k(h)^2\mathbf{D}^2_{(0)} = \tilde{\mathbf{d}}^{(1)}_x\tilde{\mathbf{d}}^{(0)}_x + \tilde{\mathbf{d}}^{(1)}_y\tilde{\mathbf{d}}^{(0)}_y \tag{16}$$

where

$$\tilde{\mathbf{d}}^{(0)}_\xi = \alpha_0\tilde{\mathbf{d}}^{(1)}_\xi + (1-\alpha_0)\tilde{\mathbf{d}}^{(2)}_\xi \tag{17}$$

$(\xi = x, y)$, and α_0 is a parameter such that (16) is fulfilled. For notational convenience, one writes $\tilde{\mathbf{d}}_\xi = \tilde{\mathbf{d}}^{(1)}_\xi$, to distinguish it from a new spatial difference operator $\tilde{\mathbf{d}}^{(2)}_\xi$, defined by

$$2\tilde{\mathbf{d}}^{(2)}_x f(x,y) = f(x+h/2,y+h) + f(x+h/2,y-h) - f(x-h/2,y+h) - f(x-h/2,y-h) \tag{18a}$$

$$2\tilde{\mathbf{d}}^{(2)}_y f(x,y) = f(x+h,y+h/2) + f(x-h,y+h/2) - f(x+h,y-h/2) - f(x-h,y-h/2). \tag{18b}$$

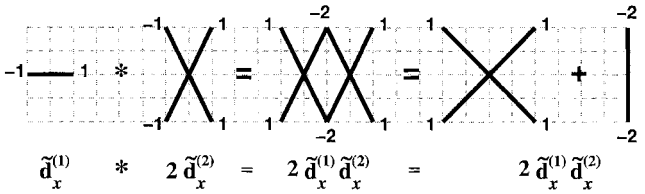

Fig. 3. Graphical depiction of two independent FD approximations ∂_x in two dimensions and their composition. Figures are centered at (x, y) and the grid spacing is $h/2$. Function values at the vertices are summed according to the indicated weight.

The operator $\tilde{\mathbf{d}}_x^{(2)}$ and $\tilde{\mathbf{d}}_x^{(1)}\tilde{\mathbf{d}}_x^{(2)}$ are depicted in Fig. 3. Using this result, it is easily shown that

$$\sum_{\xi=x,y} \tilde{\mathbf{d}}_\xi^{(1)}\tilde{\mathbf{d}}_\xi^{(2)} = 2h^2\mathbf{D}_{(2)}^2 - h^2\mathbf{D}_{(1)}^2. \tag{19}$$

Inserting (17) into (16) and solving for α_0, one finds $\alpha_0 = (1+\gamma_0)/2$.

New NSFD approximations to the space and time derivatives are now defined by

$$\mathbf{d}_\xi^{(0)} = \frac{1}{s_k(h)}\tilde{\mathbf{d}}_\xi^{(0)} \tag{20a}$$

$$\mathbf{d}_t^{(0)} = \frac{1}{s_\omega(\Delta t)}\tilde{\mathbf{d}}_t. \tag{20b}$$

Notice that in (20a), $s_k(h)$ does not depend on θ.

VI. High-Accuracy Realization of the Yee Algorithm

A high-accuracy version of the Yee algorithm can now be constructed. First, replace all the time derivatives in (4) by $\mathbf{d}_t^{(0)}$, and then replace the spatial derivatives in (4a) and (4b) by the $\mathbf{d}_\xi^{(0)}$. Finally, replace the spatial derivatives in (4c) by $\tilde{\mathbf{d}}_\xi/s_k(h)$. This yields

$$\tilde{\mathbf{d}}_t H_x\left(x, y-\frac{h}{2}, t\right) = \frac{-1}{\mu(\mathbf{x})}u(\mathbf{x})\tilde{\mathbf{d}}_y^{(0)}E_z\left(x, y-\frac{h}{2}, t\right) \tag{21a}$$

$$\tilde{\mathbf{d}}_t H_y\left(x-\frac{h}{2}, y, t\right) = \frac{1}{\mu(\mathbf{x})}u(\mathbf{x})\tilde{\mathbf{d}}_x^{(0)}E_z\left(x-\frac{h}{2}, y, t\right) \tag{21b}$$

$$\tilde{\mathbf{d}}_t E_z\left(x, y, t+\frac{\Delta t}{2}\right) = \frac{1}{\varepsilon(\mathbf{x})}u(\mathbf{x})\left[\tilde{\mathbf{d}}_x H_y\left(x, y, t+\frac{\Delta t}{2}\right) - \tilde{\mathbf{d}}_y H_x\left(x, y, t+\frac{\Delta t}{2}\right)\right] \tag{21c}$$

where $u(\mathbf{x}) = s_\omega(\Delta t)/s_{k(\mathbf{x})}(h)$, and $k(\mathbf{x}) = \omega\sqrt{\varepsilon(\mathbf{x})\mu(\mathbf{x})}$. If one sets $u(\mathbf{x}) = \Delta t/h$ and $\tilde{\mathbf{d}}_\xi^{(0)} = \mathbf{d}_\xi$, the standard Yee algorithm is recovered.

VII. Error and Stability

The solution error of algorithm (21) with respect to E_z [see Fig. 1(b)] is less than 10^{-4} of (5). At $\lambda/h = 8$, (21) yields the same accuracy as the standard Yee algorithm does at $\lambda/h = 1140$. Since both α_0 and u are functions of k, solution error is minimized only at the angular frequency ω, at which the $\mathbf{d}_\xi^{(0)}$ are defined. For nonmonochromatic signals, one might, therefore, expect that accuracy can be high only near this frequency. It turns out, however, that while solution error does increase away from ω, it is still smaller than that of algorithm (5), and is still highly isotropic. The tradeoffs needed to handle multiple frequencies are discussed in [3]. It should be noted that the solution error of the standard algorithm is also both frequency-dependent and anisotropic.

Due to the asymmetric decomposition of $\mathbf{D}_{(0)}^2$ in (16), high-accuracy solutions for both $\mathbf{E}$ and $\mathbf{H}$ are not obtained within the same computational run. Because the $\mathbf{H}$-fields are computed first, they contain an anisotropic scale error. To obtain the $\mathbf{H}$-fields with high accuracy, one could either rearrange the algorithm to compute $\mathbf{H}$ last, or compute it from the high-accuracy $\mathbf{E}$-fields in an extra computational step.

Although the accuracy of the FD approximations are improved with respect to the periodic electromagnetic-field components, such quantities are not necessarily approximated as $\partial_x\varepsilon(\mathbf{x})$ any more accurately with NSFD operators.

Stability analysis [4] for the Yee algorithm is carried out assuming a uniform sourceless medium. The stability criteria are, thus, the same as for the FDTD algorithm used to solve the wave equation [3], [7]. For algorithm (5), the stability criteria can be expressed in the form

$$\frac{\lambda/h}{T/\Delta t} \le \frac{\sqrt{2}}{2} \approx 0.70 \tag{22}$$

where T is the wave period, while for (21) one has [3]

$$\frac{\lambda/h}{T/\Delta t} \le \frac{3}{\pi}\arcsin\left(\frac{3}{4}\right) \approx 0.80. \tag{23}$$

Thus, for a fixed value of λ/h, (21) requires fewer iterations because the ratio $T/\Delta t$ can be smaller. Although, rigorously speaking, (22) and (23) are valid only for uniform, nonconducting, sourceless media, they seem to hold for the general case too [4].

VIII. Extension to Three Dimensions

In three dimensions there are three basic second-order FD Laplacians, which are graphically defined in Fig. 4. As shown in [3], one can combine them to construct an isotropic FD Laplacian of the form

$$\mathbf{D}_{(0)}^2 = \eta_1\mathbf{D}_{(1)}^2 + \eta_2\mathbf{D}_{(2)}^2 + \eta_3\mathbf{D}_{(3)}^2 \tag{24}$$

where $\eta_1 + \eta_2 + \eta_3 = 1$. Setting $(k_x, k_y, k_z) = k(\sin\theta\cos\phi, \sin\theta\sin\phi, \cos\theta)$, where θ and ϕ are spherical coordinates, one defines

$$D_1(k,\theta,\phi) = \cos k_x + \cos k_y + \cos k_z - 3 \tag{25a}$$

$$D_2(k,\theta,\phi) = \cos k_x \cos k_y \cos k_z - 1 \tag{25b}$$

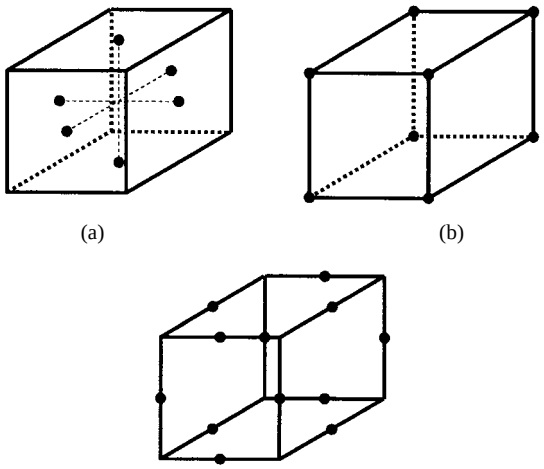

Fig. 4. Graphical depiction of three independent FD approximations to the Laplacian in three dimensions. Figures are centered at (x, y, z). Grid spacing is $h/2$. Function values at the vertices are summed according to the indicated weight.

$$D_3(k,\theta,\phi) = \frac{1}{2}(\cos k_x \cos k_y + \cos k_x \cos k_z + \cos k_y \cos k_z - 3) \tag{25c}$$

$D_{12} = \gamma_0 D_1 + (1-\gamma_0) D_2$, $D_{13} = (2\gamma_0 - 1) D_1 + 2(1-\gamma_0) D_3$, and

$$\eta_0(k) \equiv \frac{D_{13}(k, \pi/4, \phi_0) - (\cos k - 1)}{D_{13}(k, \pi/4, \phi_0) - D_{12}(k, \pi/4, \phi_0)} \tag{26}$$

where $\phi_0 = 0.118\,11\pi$. It can then be shown [3] that

$$\eta_1 = \eta_0(1-\gamma_0) + (2\gamma_0 - 1) \tag{27a}$$
$$\eta_2 = \eta_0(1-\gamma_0), \tag{27b}$$
$$\eta_3 = 1 - (\eta_1 + \eta_2). \tag{27c}$$

$\mathbf{D}^2_{(0)}$ is now decomposed in the form

$$s_k(h)^2 \mathbf{D}^2_{(0)} = \tilde{\mathbf{d}}^{(1)}_x \tilde{\mathbf{d}}^{(0)}_x + \tilde{\mathbf{d}}^{(1)}_y \tilde{\mathbf{d}}^{(0)}_y + \tilde{\mathbf{d}}^{(1)}_z \tilde{\mathbf{d}}^{(0)}_z \tag{28}$$

where

$$\tilde{\mathbf{d}}^{(0)}_\xi = \alpha_1 \tilde{\mathbf{d}}^{(1)}_\xi + \alpha_2 \tilde{\mathbf{d}}^{(2)}_\xi + \alpha_3 \tilde{\mathbf{d}}^{(3)}_\xi \tag{29}$$

$\tilde{\mathbf{d}}^{(1)}_\xi = \tilde{\mathbf{d}}_\xi$, and $\tilde{\mathbf{d}}^{(2)}_\xi$ and $\tilde{\mathbf{d}}^{(3)}_\xi$ are new difference operators, and the α satisfy the constraint $\alpha_1 + \alpha_2 + \alpha_3 = 1$. In Fig. 5 one graphically defines $\tilde{\mathbf{d}}^{(1)}_x$, $\tilde{\mathbf{d}}^{(2)}_x$, and $\tilde{\mathbf{d}}^{(3)}_x$. Rotating the coordinate axes relative to the figures, one can easily infer the definitions of the other spatial difference operators. Following the graphical computation of Fig. 3, one can easily show that

$$\sum_{\xi=x,y,z} \tilde{\mathbf{d}}^{(1)}_\xi \tilde{\mathbf{d}}^{(2)}_\xi = h^2(3\mathbf{D}^2_{(2)} - 2\mathbf{D}^2_{(3)}) \tag{30a}$$
$$\sum_{\xi=x,y,z} \tilde{\mathbf{d}}^{(1)}_\xi \tilde{\mathbf{d}}^{(3)}_\xi = h^2(2\mathbf{D}^2_{(3)} - \mathbf{D}^2_{(1)}). \tag{30b}$$

Inserting (29) into (28) and using (30) one finds

$$\alpha_1 = \eta_1 + \frac{1}{3}\eta_2 + \frac{1}{2}\eta_3 \tag{31a}$$

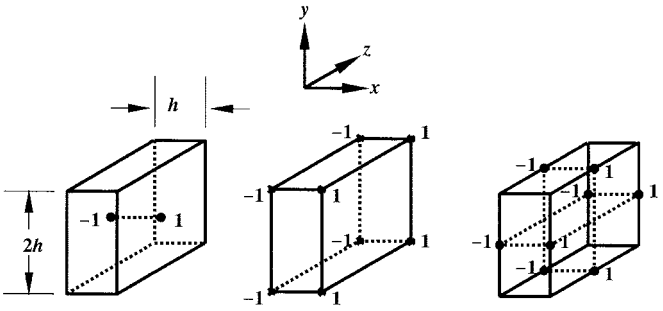

Fig. 5. Graphical depiction of three different FD approximations to ∂_x in three dimensions. Figures are centered at (x, y, z) and the grid spacing is $h/2$. Function values at the vertices are summed according to the indicated weight.

$$\alpha_2 = \frac{1}{3}\eta_2 \tag{31b}$$
$$\alpha_3 = \frac{1}{3}\eta_2 + \frac{1}{2}\eta_3. \tag{31c}$$

NSFD's are now substituted into Maxwell's equations to obtain a high-accuracy Yee algorithm. Following Section VI, the time derivatives in (3) are replaced by $\mathbf{d}^{(0)}_t$, the spatial derivatives in (3a) by the $\mathbf{d}^{(0)}_\xi$, and those in (3b) by $\tilde{\mathbf{d}}_\xi / s_k(h)$ to obtain

$$\tilde{\mathbf{d}}_t H_x\left(x, y-\frac{h}{2}, z-\frac{h}{2}, t\right) = \frac{-u(\mathbf{x})}{\mu(\mathbf{x})}\left[\tilde{\mathbf{d}}^{(0)}_y E_z\left(x, y-\frac{h}{2}, z-\frac{h}{2}, t\right) - \tilde{\mathbf{d}}^{(0)}_z E_y\left(x, y-\frac{h}{2}, z-\frac{h}{2}, t\right)\right] \tag{32a}$$

$$\tilde{\mathbf{d}}_t H_y\left(x-\frac{h}{2}, y, z-\frac{h}{2}, t\right) = \frac{-u(\mathbf{x})}{\mu(\mathbf{x})}\left[\tilde{\mathbf{d}}^{(0)}_z E_x\left(x-\frac{h}{2}, y, z-\frac{h}{2}, t\right) - \tilde{\mathbf{d}}^{(0)}_x E_z\left(x-\frac{h}{2}, y, z-\frac{h}{2}, t\right)\right] \tag{32b}$$

$$\tilde{\mathbf{d}}_t H_z\left(x-\frac{h}{2}, y-\frac{h}{2}, z, t\right) = \frac{-u(\mathbf{x})}{\mu(\mathbf{x})}\left[\tilde{\mathbf{d}}^{(0)}_x E_y\left(x-\frac{h}{2}, y-\frac{h}{2}, z, t\right) - \tilde{\mathbf{d}}^{(0)}_y E_x\left(x-\frac{h}{2}, y-\frac{h}{2}, z, t\right)\right] \tag{32c}$$

$$\tilde{\mathbf{d}}_t E_x\left(x-\frac{h}{2}, y, z, t+\frac{\Delta t}{2}\right) = \frac{u(\mathbf{x})}{\varepsilon(\mathbf{x})}\left[\tilde{\mathbf{d}}_y H_z\left(x-\frac{h}{2}, y, z, t+\frac{\Delta t}{2}\right) - \tilde{\mathbf{d}}_z H_y\left(x-\frac{h}{2}, y, z, t+\frac{\Delta t}{2}\right)\right] \tag{32d}$$

$$\tilde{\mathbf{d}}_t E_y\left(x, y-\frac{h}{2}, z, t+\frac{\Delta t}{2}\right) = \frac{u(\mathbf{x})}{\varepsilon(\mathbf{x})}\left[\tilde{\mathbf{d}}_z H_x\left(x, y-\frac{h}{2}, z, t+\frac{\Delta t}{2}\right) - \tilde{\mathbf{d}}_x H_z\left(x, y-\frac{h}{2}, z, t+\frac{\Delta t}{2}\right)\right] \tag{32e}$$

$$\tilde{\mathbf{d}}_t E_z\left(x,y,z-\frac{h}{2},t+\frac{\Delta t}{2}\right) = \frac{u(\mathbf{x})}{\varepsilon(\mathbf{x})}\left[\tilde{\mathbf{d}}_x H_y\left(x,y,z-\frac{h}{2},t+\frac{\Delta t}{2}\right) - \tilde{\mathbf{d}}_y H_x\left(x,y,z-\frac{h}{2},t+\frac{\Delta t}{2}\right)\right]. \tag{32f}$$

Again, the standard Yee algorithm can be recovered by setting $u(\mathbf{x}) = \Delta t/h$ and $\mathbf{d}_\xi^{(0)} = \mathbf{d}_\xi$.

The solution error follows from the discussion in [3], [4]. Fig. 1 depicts the solution error for the standard and nonstandard Yee algorithms in three dimensions with respect to θ. It is of similar magnitude with respect to ϕ.

Following [3], [4], the stability criterion for the standard three-dimensional (3-D) Yee algorithm can be expressed in the form

$$\frac{\lambda/h}{T/\Delta t} \le \frac{\sqrt{3}}{3} \approx 0.57 \tag{33a}$$

while for the high-accuracy version (32), one has

$$\frac{\lambda/h}{T/\Delta t} \le \frac{3}{\pi}\arcsin\left(\sqrt{\frac{15}{23}}\frac{\sqrt{3}}{2}\right) \approx 0.73. \tag{33b}$$

Since the value on the left in (33b) is larger than in (33a), fewer time steps are required for the NSFD Yee algorithm than for the ordinary one.

Again, as in the 2-D case, high accuracy is obtained only for the $\mathbf{E}$-fields. To obtain the $\mathbf{H}$-fields with equal accuracy, one could either rearrange the algorithm to compute $\mathbf{H}$ last, or compute it from the $\mathbf{E}$-fields.

IX. Parallel Program Realizations and Visualizations

By extending the author's previous work [5], [6], both the standard and high-accuracy Yee algorithms in parallel FORTRAN-90 code have been implemented. The high-accuracy version can be realized by simple modifications of the basic Yee code. The field components, medium parameters, and $u(\mathbf{x})$ and $\alpha_0(\mathbf{x})$ are represented as 2-D or 3-D arrays. The $\mathbf{E}(\mathbf{x},t)$- and $\mathbf{H}(\mathbf{x},t)$-arrays are updated at every time step. Current sources and conducting media can be accommodated by appropriate modifications [4] of (21) or (32). Time varying, moving media, and moving sources can be incorporated by updating the appropriate arrays at every time step. Our core program is about one page of FORTRAN-90 code.

By displaying one or more wave fields per wave period, movie-like visualizations of time-dependent electromagnetic wave propagation and scattering processes are created, which can be viewed on line while the calculation is actually running. This obviates the need to store large quantities of data, and gives a heuristic feel for the calculation. An example application to Mie scattering off of a dielectric, which cannot be performed analytically is shown in Fig. 6.

X. Summary and Conclusion

New NSFD's have been introduced to construct a high-accuracy FDTD algorithm to solve Maxwell's equations, which are some 10 000 times more accurate than the standard Yee algorithm. At $\lambda/h = 8$, the same accuracy is achieved as the standard Yee algorithm achieves at $\lambda/h = 1140$. The highest accuracy is achieved at one fixed frequency, but it is possible to handle moderate bandwidths with some tradeoffs. The computational load per grid point is greater, but it is more than offset by the low λ/h ratio which can be used, as well as by a decrease in the number of iterations needed. High accuracy is achieved by using all 27 grid points in a $3 \times 3 \times 3$ region. This compact computational molecule is well suited to parallel and distributed computing platforms.

Fig. 6. 2-D Mie scattering. Gaussian TM wave (E_z normal–to–paper) scatters off two rotated ellipses. E_z amplitude is depicted. Spatial grid is $\lambda/h = 8$, while the time gridding is $T/\Delta T = 12$, where λ and T are the wavelength and wave period, respectively. Ellipse major and minor axes are 2λ and 4λ, respectively.

Acknowledgment

The author wishes to thank his colleagues at the Naval Research Laboratory for their help and advice, particularly Dr. R. Krutar for the seminal remark that sparked this line of investigation, Dr. S. Numrich, who introduced him to supercomputing, and Dr. L. Schuette for his help and encouragement. The author also thanks the NRL Connection Machine staff, particularly J. Osburne for invaluable technical advice, the Physical Research Institute (RIKEN) in Japan, where some of this work began, and the University of Tsukuba, Japan, for their generous support.

References

[1] K. S. Yee, "Numerical solution of initial boundary value problems involving Maxwell's equations in isotropic media," *IEEE Trans. Antennas Propagat.*, vol. AP-14, pp. 302–307, May 1966.

[2] R. E. Mickens, *Nonstandard Finite Difference Models of Differential Equations.* Singapore: World Scientific, 1984.

[3] J. B. Cole, "A high-accuracy FDTD algorithm to solve microwave propagation and scattering problems on a coarse grid," *IEEE Trans. Microwave Theory Tech.*, vol. 43, pp. 2053–2058, Sept. 1995.

[4] R. C. Booton, *Computational Methods for Electromagnetics and Microwaves*. New York: Wiley, 1992.
[5] J. B. Cole, R. Krutar, D. B. Creamer, and S. K. Numrich, "Finite-difference time-domain simulations of wave propagation and scattering as a research and educational tool," *Comput. in Physics*, Apr.–May 1995.
[6] S. K. Numrich, R. A. Krutar, and R. Squier, "Computation of acoustic fields on a massively parallel processor using lattice gas methods, in computational acoustics," R. D. Lau *et al.*, Eds., in *Proc. 3rd IMACS Symp.* 1991.
[7] S. K. Godunov, *Difference Schemes*. Amsterdam, The Netherlands: North Holland, 1987.

James B. Cole (M'89) received the B.S. degree in physics from the Illinois Institute of Technology, Chicago, the M.S. degree in information engineering from the University of Illinois–Chicago, and the Ph.D. degree in elementary particle physics from the University of Maryland, College Park, in 1972, 1981, and 1987, respectively. He also studied low-temperature physics at the Institute for Applied Physics, University of Hamburg, Germany, in 1982.

He was a National Research Council Post-Doctoral Fellow at the Laboratory for High Energy Astrophysics, NASA Goddard Space Flight Center, Washington, D.C., in 1988. Afterwards, he joined the staff of the Army Research Laboratory, and in 1990 transferred to the Naval Research Laboratory, Washington, D.C., to work on parallel computing and physical simulations. He was a Visiting Professor in 1990 at the NTT Basic Research Laboratory, Japan, and in 1994 was a Visiting Scientist at the Physical-Chemical Research Institute (RIKEN), Japan. He is presently at the University of Tsukuba, Tsukuba, Japan. His current research is the simulation and visualization of physical phenomena in the interdisciplinary areas of electrical engineering, applied physics, and applied mathematics.